JACS
JOURNAL OF THE AMERICAN CHEMICAL SOCIETY

ARTICLE

pubs.acs.org/JACS

Dramatic Structural Rearrangements in Porous Coordination Networks

Javier Martí-Rujas,[†,#] Nazrul Islam,[∥] Daisuke Hashizume,[‡] Fujio Izumi,[§] Makoto Fujita,[†] and Masaki Kawano*[,∥]

[†]Department of Applied Chemistry, School of Engineering, The University of Tokyo, Hongo, Bunkyo-ku, Tokyo 113-8656, Japan

[‡]Advanced Technology Support Division, RIKEN, Hirosawa, Wako, Saitama 351-0198, Japan

[§]Quantum Beam Center, National Institute for Materials Science, 1-1 Namiki, Tsukuba, Ibaraki 305-0044, Japan

[∥]The Division of Advanced Materials Science, Pohang University of Science and Technology (POSTECH), San 31 Hyojadong, Pohang 790-784, Korea

Supporting Information

ABSTRACT: With the use of *ab initio* X-ray powder diffraction, a family of isostructural crystalline porous coordination networks, $[(ZnX_2)_3(TPT)_2]_n \cdot$ (solvent) (X = I, Br, Cl), has been studied at elevated temperatures of 573−723 K. Upon heating, all three networks exhibited crystalline-to-amorphous-to-crystalline (CAC) phase transformations to three new networks, $[(ZnI_2)_3(TPT)_2]_n$, $[(ZnBr_2)_3(TPT)_2]_n \cdot (H_2O)$ and $[(ZnBr_2)(\mu\text{-Br})(ZnBr)(TPT)]_n$, and $[(ZnCl_2)(\mu\text{-Cl})(ZnCl)(TPT)]_n$, respectively. A set of control experiments was used to obtain detailed mechanistic aspects of the CAC transformations. We demonstrate how bonds are broken and formed in these significant molecular rearrangements and how the initial arrangement plays a crucial role in the formation of the new networks after the CAC transformations. The structural information in the amorphous phase is retained and passed from a metastable to a more stable crystal, thus, reinforcing the notion that coordination networks are flexible and chemically active.

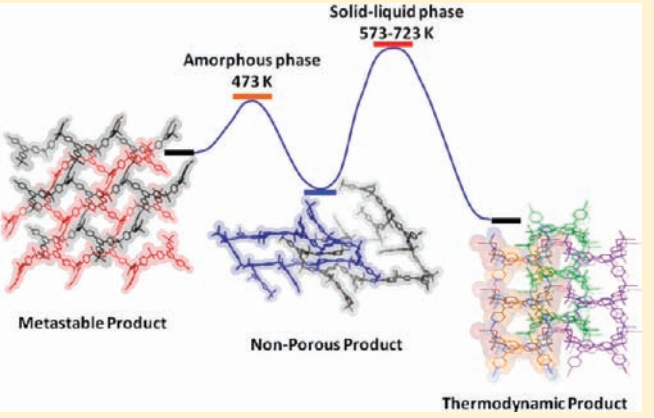

INTRODUCTION

Porous coordination networks are extremely versatile materials due to the hybrid nature of their constituent building blocks (i.e., metal ions and organic ligands), which allows them to be used in applications such as conductivity, catalysis, and gas adsorption.[1−9] The formation of thermodynamically stable porous coordination networks is crucial for their potential applications. Depending on the crystallization conditions during the self-assembling process, the resulting porous coordination networks can be stable thermodynamic products or metastable kinetic products. Thermodynamically controlled porous coordination networks can be obtained via conventional self-assembly methods in solution over long periods of time (i.e., days to weeks).[10−12] The resulting stable products yield crystals that can be readily determined by single crystal X-ray diffraction and, in particular cases, single-crystal-to-single-crystal (SCSC) reactions allow solid-state reactions to be studied in detail.[13−16] Conversely, metastable products are more difficult to be characterized by single crystal X-ray diffraction due to their small crystal size resulting from fast crystallization process and due to their tendency to transform into more stable structures.[17]

One of the primary problems chemists face in studying solid-state reactions is that often the single crystals transform into poly-microcrystalline samples and therefore are not suitable for structural characterization by single-crystal X-ray diffraction. For this reason, there are many solid-state chemical reactions that remained unexplored. However, thanks to recent advances in *ab initio* structure determination by X-ray powder diffraction (XRPD),[18−26] chemical reactions can be characterized in detail in a single-crystal-to-polycrystalline manner.

Solid-state reactions involving intermediate amorphous phases are challenging, yet fascinating reactions because they can form new materials that are difficult (if not impossible) to be obtained from solution, providing that the solid-state reactions have different reaction conditions to those in the solution state.[27]

In this regard, we recently reported how a double interpenetrated porous coordination network $[(ZnI_2)_3(TPT)_2]_n \cdot 5.5(C_6H_5NO_2)(H_2O)$ (**1**), where TPT is tris(4-pyridyl)triazine, transforms into the remarkably stable porous network $[(ZnI_2)_3(TPT)_2]_n$ (**1a**) in a solid-state reaction at high temperatures exceeding 573 K.[28] The reaction occurs via a crystalline-to-amorphous-to-crystalline (CAC) phase transformation that involves significant

Received: October 19, 2010
Published: March 25, 2011

dx.doi.org/10.1021/ja109160a | J. Am. Chem. Soc. 2011, 133, 5853–5860

molecular rearrangements. From those results, it seems that the initial arrangement of molecules within metastable structure (**1**) can play an important role in the synthesis of new crystal structures. To gain insights in the mechanistic aspects of such CAC phase transformations, we exploited state-of-the-art methods for structure determination from powder X-ray diffraction data to study a set of isostructural metastable coordination networks $[(ZnBr_2)_3(TPT)_2]_n \cdot 5(C_6H_5NO_2)(H_2O)$ (**2**) and $[(ZnCl_2)_3(TPT)_2]_n \cdot 5.5(C_6H_5NO_2)(H_2O)$ (**3**) at elevated temperatures. We found that the metastable structures (**1**−**3**) undergo CAC phase transformation involving bond-breaking and bond-forming to yield three new stable products. Furthermore, we studied the role of the intermediate amorphous phase in order to elucidate whether a structural memory effect exists during the CAC transformations. In addition to size difference in halides, the difference in strength of Zn−halide coordination bonds in the metastable structures plays a crucial role in the final structures.

Scheme 1. Porous Coordination Networks, 1, 2, and 3 Synthesized Using the "Instant Synthesis" Method

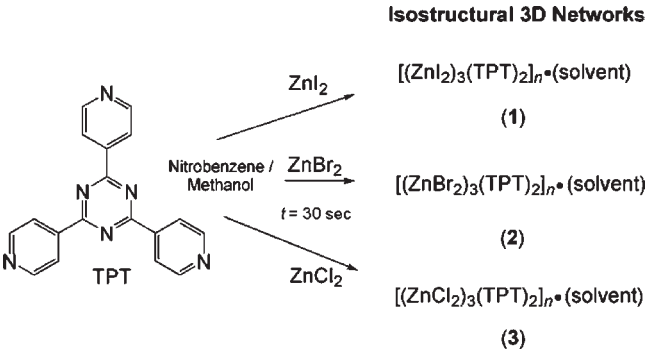

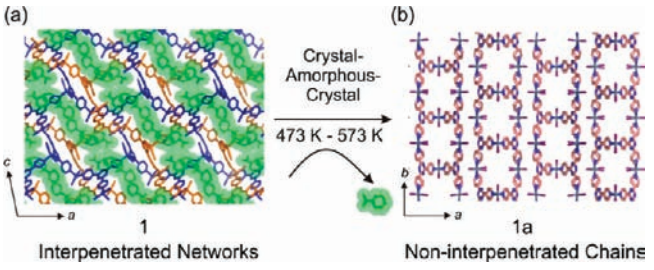

Figure 1. Crystal structure transformation from **1** to **1a**. (a) In **1**, the two interpenetrating networks are shown in blue and orange, while nitrobenzene guest molecules are in green. (b) In **1a**, there is no network interpenetration and the porous structure is maintained without guest molecules filling the pores. Compound **1a** is stable up to 623 K.

RESULTS AND DISCUSSION

Synthesis of Metastable Interpenetrated Networks 1, 2, and 3. Kinetically controlled metastable compounds **1**, **2**, and **3** were synthesized using the "instant synthesis" method (Scheme 1).[29] A fine homogeneous powder of **1** was obtained by instant mixing of ZnI_2 (0.24 mmol) with TPT (0.16 mmol) in an 8:1 nitrobenzene/methanol solution (36 mL) within 30 s. Compounds **2** and **3** were obtained using the same method but replacing ZnI_2 with $ZnBr_2$ and $ZnCl_2$, respectively. The XRPD patterns, simulated powder patterns from single crystal structures, and elemental analyses all indicate that pure phases of **1**, **2**, and **3** were obtained.[30] Compounds **1**, **2**, and **3** are isostructural and are described as double interpenetrated (10,3-*b*) networks.[31] The shortest circuit within the networks is composed of 10 Zn halides and 10 TPT molecules.[32] Thermogravimetric analysis and differential scanning calorimetry (TG-DSC) experiments show that all three structures gradually release solvent between 300 and 500 K (See Supporting Information).

Thermodynamic Stability and Structural Properties of 1. Upon heating from 300 to 673 K, compound **1** (Figure 1a) undergoes a CAC transformation.[28] In situ XRPD shows that **1** changes to an amorphous phase at 473 K and upon further heating a new crystalline porous phase (**1a**) appears uniformly at 573 K and is stable up to 673 K (Figure 1b). TG-DSC experiments revealed that after the release of solvent molecules a new crystalline phase is obtained as indicated by the exothermic peak at ca. 573 K (Figure S1).

Importantly, the metal-to-ligand ratio (M/L) of 3:2 in **1a** remains unchanged throughout the reaction. The stability of **1a** was studied under vacuum conditions and low temperature (95 K).[33,34] The XRPD data demonstrates that **1a** is stable under those conditions. Direct *ab initio* structure solution[18−20] indicates that the framework in **1a** under vacuum is the same as the one at atmospheric pressure, with only a small distortion of the ligand TPT. Guest inclusion behavior of **1a** was demonstrated by immersion of **1a** in nitrobenzene.[28] Because of the potential

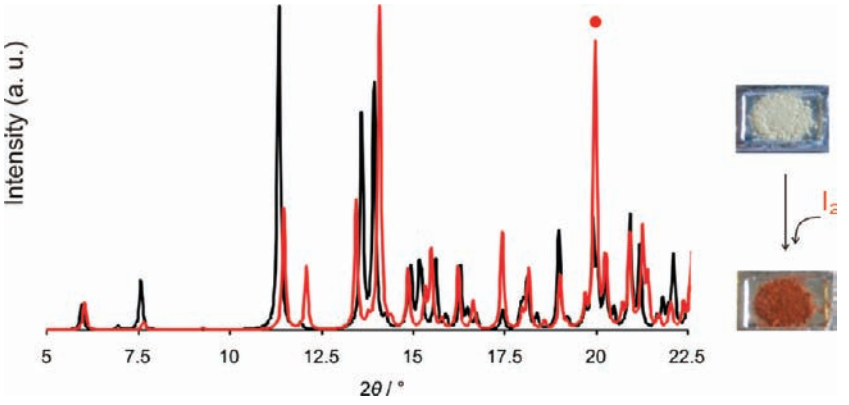

Figure 2. Simulated XRPD patterns of **1a** (black) and $\mathbf{1a \cdot G_1}$ (red) obtained from *ab initio* structure solution. The peak at ca. $2\theta \approx 19°$ (red circle) corresponds to the 22-1 *hkl* plane which contains the I_2 molecule in the pore (wavelength used for simulation, λ = 1.5406 Å).

dx.doi.org/10.1021/ja109160a |*J. Am. Chem. Soc.* 2011, 133, 5853–5860

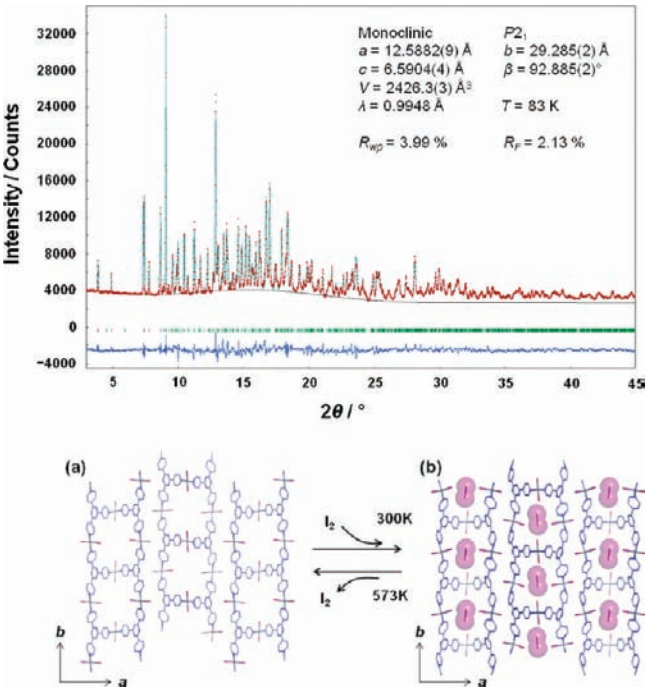

Figure 3. Experimental (red), calculated (pale-blue), and difference (dark-blue) XRPD profiles from the final Rietveld refinement of **1a**·G_1 (top). Temperature-dependent reversible guest inclusion/removal of I_2 in **1a** (bottom).

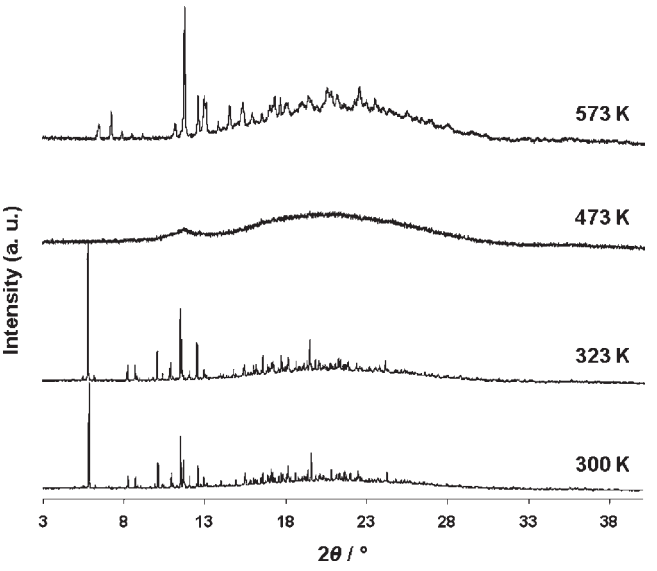

Figure 4. *In situ* synchrotron XRPD patterns of **2** measured at different temperatures. The formation of an intermediate amorphous phase at 473 K shows that significant molecular reorganization occurs during the solid-state reaction. The formation of a new crystalline phase is observed at 573 K at a heating rate 10 °C/min.

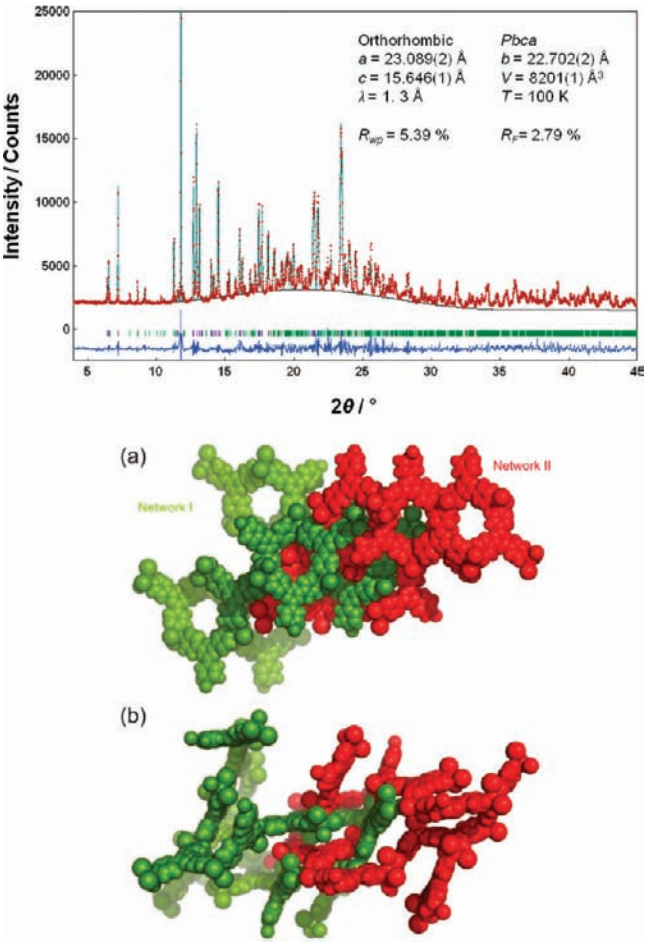

Figure 5. Experimental (red), calculated (pale-blue), and difference (dark-blue) XRPD profiles from the final Rietveld refinement of **2a** (top). Crystal structure of **2a**: (a) detailed view along the *c*-axis of the two interpenetrated circuits (green and red) formed after the CAC transformation. (b) Side view of the same interpenetrated networks showing the $\pi-\pi$ stacking between TPT ligands (bottom).

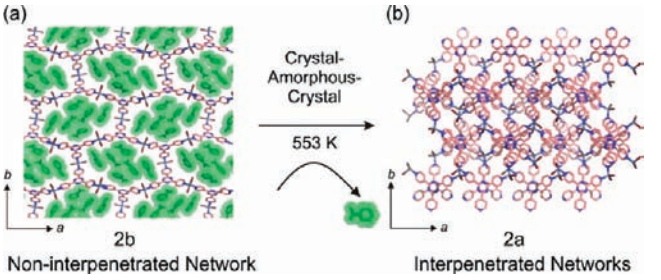

Figure 6. Structural rearrangement of the noninterpenetrated network **2b** into the interpenetrated structure of **2a** upon heating (553 K) via CAC phase transformations.

industrial applications of porous coordination networks to materials for catalysts, conductivity, chemical sensors, and so on, we were prompted to further investigate the inclusion of smaller molecules (I_2). Compound $[(ZnI_2)_3(TPT)_2 \cdot x(G_1)]_n$ (with $x = 0.6$ (**1a**·G_1), where $G_1 = I_2$) was successfully obtained by exposure of **1a** to vapors of I_2 at 300 K for 12 h. The peak shift and change in the relative intensities of the XRPD pattern suggest the inclusion of I_2 (Figure 2). In particular, the intense peak in **1a**·G_1 at $2\theta \approx 19°$, which corresponds to the *hkl* plane 22-1, indicates that I_2 is included in the pore. This is also supported by the color change from light yellow (**1a**) to brown (**1a**·G_1). The structure of **1a**·G_1 was solved directly by *ab initio* XRPD. The good agreement between experimental and calculated diffraction

dx.doi.org/10.1021/ja109160a |*J. Am. Chem. Soc.* 2011, 133, 5853–5860

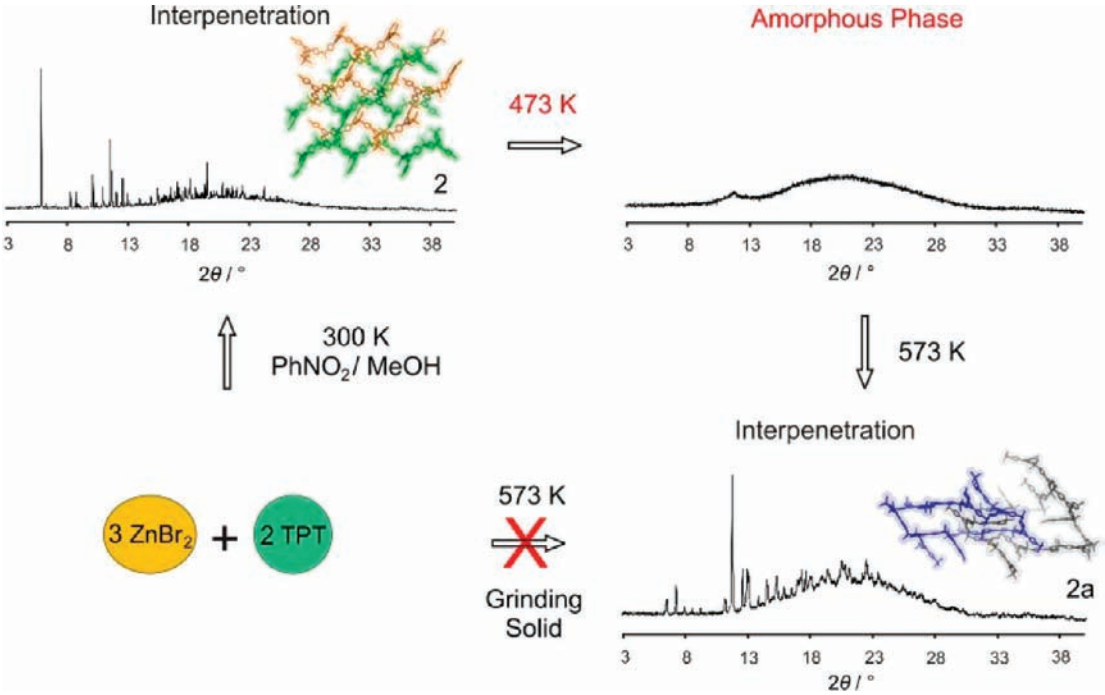

Figure 7. XRPD patterns and structures of **2** and **2a** obtained from *ab initio* XRPD. Compound **2** was transformed to **2a** in the solid-state via amorphous phase upon heating at 573 K, whereas grinding solid TPT and $ZnBr_2$ and heating to 573 K did not form **2a**.

patterns in the Rietveld refinement shows the correctness of the structure (Figure 3). The guest inclusion of I_2 is reversible since heating **1a**·$\mathbf{G_1}$ to 573 K produced **1a** again (Figure 3).

The I_2 molecules are located between iodide atoms of ZnI_2 units at the center of the pore. The intermolecular distance between I_2 molecules is 6.59 Å which suggests that there is no interaction among I_2 molecules. The dihalogen I_2 acts as Lewis acid (halogen bond donor) and the I from the ZnI_2 acts as Lewis base (halogen bond acceptor)[35−39] to form a one-dimensional array through halogen bonding interactions. One I_2 is halogen bonded to two I atoms through the I···I−I interactions (d_1 = 3.76 Å; 158° and d_2 = 3.67 Å; 174°). The attractive nature of this halogen bonding interaction is evidenced by the I···I distances that are shorter than the sum of van der Waals radii of two I atoms (3.96 Å). Unlike other compounds involving halogen bonding interactions with I_2, the I_2 in **1a**·$\mathbf{G_1}$ does not have amphoteric behavior (i.e., both termini of the I_2 act as a Lewis acid).[36] Thus, the attractive nature of the halogen bonding interaction can be considered as the main driving force for the inclusion of the I_2 in **1a**.

Retention of Structural Information through the CAC Transformation in 1. The formation of the amorphous phase can be rationalized by the significant molecular reorganization occurring during the phase transition (423 to 523 K) from double interpenetrated to the noninterpenetrated topology of **1a**. Clearly, unlocking of the two networks implies cleavage and formation of zinc−nitrogen coordination bonds. In this solid-state reaction, it is likely that a certain degree of structural memory of **1** persists in the amorphous phase (473 K) in order to form **1a**. To prove that, we carried out a control experiment by finely grinding powder of ZnI_2 and TPT (3:2 molar ratio). However, the amorphous phase obtained after grinding did not produce **1a** at 573 K (Figure S4a). Moreover, DSC experiments of a grinding mixture of ZnI_2 and TPT (3:2 molar ratio) did not show any exothermic peak upon heating to 573 K, indicating that no crystallization of **1a** occurs (Figure S4b). The same experiment but with the addition of a small amount of nitrobenzene to the mixture of ZnI_2 and ligand TPT also did not form **1a** after heating to 573 K. These experiments, where there is no prior molecular rearrangement, suggest that the preorganization in **1** is crucial for the uniform formation of **1a**. Furthermore, in order to study if the same phenomena (i.e., bond breaking and bond forming) occurred when a different type of interpenetrated porous coordination network is used as starting material, the biporous coordination network $[(ZnI_2)_3(TPT)_2(\text{triphenylene})]_n \cdot x(C_6H_5NO_2) \cdot y(CH_3OH)$ (where $x \approx 4$ and $y \approx 2$) (**1b**)[40] was heated at 573 K. Interestingly, PXRD analysis shows that the same thermodynamically stable structure **1a** is obtained (Figures S5 and S6).

Crystalline-to-Amorphous-to-Crystalline Phase Transition and Structural Properties of 2: Structural Memory Effect and High Temperature Synthesis of Bromide-Bridged M_2L Network. Microcrystalline powder of **2** was heated to 573 K in the hot stage of the diffractometer and monitored by *in situ* XRPD analysis. The diffraction data shows two phase transitions through a CAC process (Figure 4). After annealing **2** in air at 573 K for 36 h, a highly polycrystalline solid was obtained and confirmed by DSC from the exothermic peak at ca. 540 K (Figure S2). We noted that the same XRPD pattern was obtained at lower temperatures (i.e., 543−573 K).[29] Elemental analysis suggests that the compound is $[(ZnBr_2)_3(TPT)_2]_n \cdot (H_2O)$ (**2a**). High quality synchrotron XRPD data of **2a** was recorded and structure determination was carried out by *ab intio* XRPD followed by Rietveld refinement (Figure 5). The compound **2a** is a double interpenetrated network obtained after nitrobenzene guest removal and molecular rearrangement (Figure 5). The significant molecular reorganization of the framework, which can be explained by the formation of the amorphous phase, resulted in loss of single crystallinity, a large unit cell volume reduction of 47%, and change in the crystal system from monoclinic to orthorhombic.

dx.doi.org/10.1021/ja109160a |*J. Am. Chem. Soc.* 2011, 133, 5853–5860

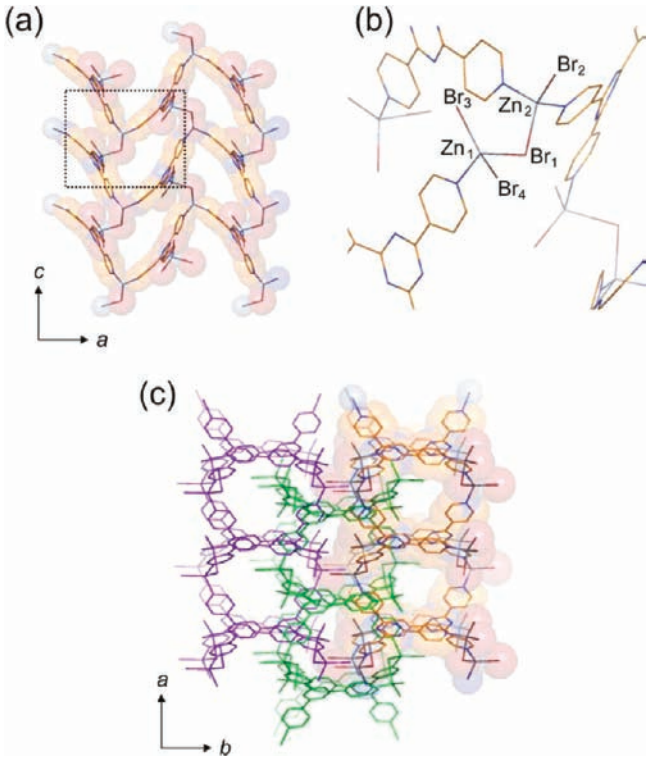

Figure 8. Single crystal structure of **2c**. (a) Sheet showing the link among "saddle units" expanding through the plane *ac*. (b) Detailed side view image of the new coordination motif between the Br and the Zn atoms. (c) Three intercalated sheets (purple, green, and color coded) showing porosity. Color code: C, orange; Zn, gray; N, blue; and Br, brown.

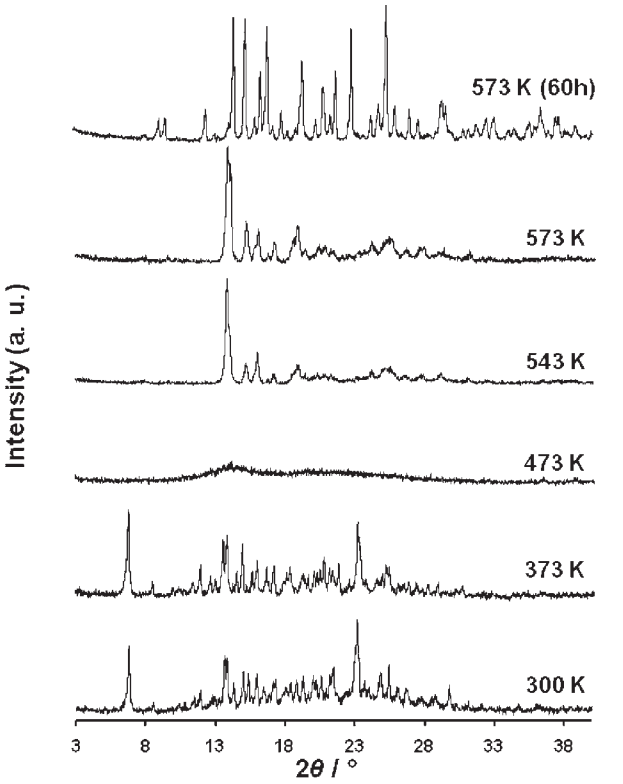

Figure 9. *In situ* XRPD patterns of **3** measured at different temperatures. The formation of an intermediate amorphous phase at 473 K shows that severe molecular reorganization takes place during the solid-state reaction. The formation of a new crystalline phase (**3a**) (i.e., similar to that of **2a**) is observed at 573 K. Annealing **3a** for 60 h with a heating rate 10 °C/min generated a new compound **3b**.

Regarding the topology, like in **1** and **2**, the shortest circuit observed in **2a** consists of 10 molecules of TPT and 10 Zn atoms. One single circuit forms channels along the *c*-axis (Figure 5a). However, in the absence of guests to fill up the channels, a second circuit interpenetrates through $\pi-\pi$ stacking interactions and forms a nonporous double interpenetrated network (Figure 5b).

It is important to elucidate whether there is cleavage and formation of coordination bonds and whether retention of structural features exists through the amorphous transition. Although the similar double interpenetration connectivity between **2** and **2a** is observed, the above structural changes and the presence of amorphous phase during the heating process suggest that the molecular reorganization in **2** should involve cleavage and formation of coordination bonds. To clarify this aspect, we investigated the network $[(ZnBr_2)_3(TPT)_2]_n \cdot 6(C_6H_5NO_2)$ (**2b**), which is a noninterpenetrated network having 1D channels (diameter: ca. 25 Å) (Figure 6a).[29] Heating **2b** to 553 K yields the same XRPD pattern of compound **2a** (Figure S10) and therefore the same crystal structure (Figure 6b).[41] Clearly, this evidence proves that cleavage and formation of coordination bonds must occur during the CAC transformation from **2b** (noninterpenetrated) to **2a** (interpenetrated). To understand the role of the amorphous intermediate phase more clearly, we carried out two control experiments. First, we mixed $ZnBr_2$ and TPT powder in a 3:2 molar ratio, ground and heated to 573 K for 36 h. However, XRPD data demonstrated that compound **2a** was not formed. Moreover, TG-DSC experiments showed no exothermic peak between 550 and 580 K, indicating that no crystallization of **2a** took place (Figure S12). Similarly to the CAC transformation of **1** into **1a**, the above results show that the molecular prearrangement in **2** and **2b** is necessary to form **2a**. Therefore, a certain degree of structural features remains in the amorphous phase (i.e., a sort of memory effect) that permits structural information to be propagated from the metastable structure toward a more stable network **2a** (Figure 7).

To study if breaking of the interpenetration in **2a** and formation of a new network was possible, **2a** was heated in air to 723 K for 4 h in a furnace. After cooling down to 300 K over 36 h, single crystals suitable for X-ray analysis were obtained. Single crystal X-ray analysis revealed new bromide-bridged coordination network $[(ZnBr_2)(\mu\text{-}Br)(ZnBr)(TPT)]_n$ (**2c**) (Figure 8). The metal-to-ligand ratio changed from M_3L_2 to M_2L during this process. The new three-dimensional network (**2c**) has two TPT ligands connected through one $ZnBr_2$. Because of local changes in the coordination environment, one of the two Zn atoms has a tetrahedral geometry through coordination to three Br and one pyridyl group (Figure 8b). The bridging coordination bond extends two-dimensionally along the *a*- and *c*-axes directions and forms layers (Figure 8a). Each layer can be regarded as a porous structure. However, adjacent two-dimensional layers are not interpenetrated but rather intercalated, and therefore, the intrinsic porosity of each layer is lost upon stacking (Figure 8c).

Crystalline-to-Amorphous-to-Crystalline Phase Transition and Structural Properties of 3: High Temperature Synthesis of Chloride-Bridged M_2L Network. Deliberately, we synthesized the metastable interpenetrated network $[(ZnCl_2)_3(TPT)_2]_n \cdot 5.5(C_6H_5NO_2)(CH_3OH)(H_2O)$ (**3**) homogeneously

dx.doi.org/10.1021/ja109160a |*J. Am. Chem. Soc.* 2011, 133, 5853–5860

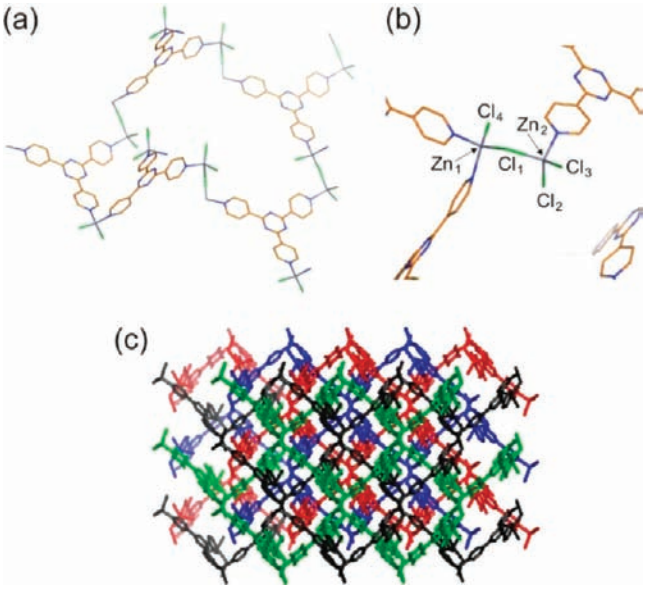

Figure 10. Single crystal structure of **3b**. (a) Shortest circuit composed of TPT and Zn in **3b**. (b) Detailed coordination environment around the Zn_1 and Zn_2 atoms. (c) Side view showing the interpenetration between the networks. Color code (top): C, orange; Zn, gray; N, blue; and Cl, green.

by using the instant synthesis method. X-ray structure determination, elemental analysis, and thermogravimetric studies revealed that compound **3** was isostructural to **1** and **2**.[42] Similarly to **1** and **2**, a CAC phase transition of **3** during heating at 573 K was observed. Note that the diffraction pattern observed at 573 K was similar to that of **2a**. This observation indicates the presence of a nonporous desolvated structure (i.e., namely **3a**).[43] However, the powder **3a** was not as stable as **2a**, so that successive 60 h annealing at 573 K produced a new powder pattern (Figure 9).

Interestingly, further annealing of **3** in a furnace at 723 K for 4 h and subsequently cooling to 300 K over 36 h produced single crystals suitable for X-ray crystallography. Single crystal X-ray crystallographic analysis revealed the formation of a new structure $[(ZnCl_2)(\mu\text{-}Cl)(ZnCl)(TPT)]_n$ (**3b**). The simulated XRPD pattern from single crystal data reasonably matched the diffraction pattern of the product obtained at 573 K (Figures S18 and S19). The TG-DSC analysis revealed that **3** gradually releases nitrobenzene first at temperatures from 300 to 500 K, followed by the formation of phase **3b** as evidenced by the exothermic peak around 525 K (Figure S3).

As in **2c**, the metal-to-ligand ratio in **3b** also changed from M_3L_2 to M_2L during this process. One Zn metal coordinates to three Cl atoms and one pyridyl group, while the second Zn atom coordinates to two Cl and two pyridyl groups (Figure 10); thus, both Zn centers adopt a tetrahedral geometry. Compound **3b** is a two-fold interpenetrated network in which each network forms a square channel. However, the channels are no longer present due to the interpenetration of individual networks. Despite having the bridging motif between the Zn and Cl atoms, **3b** is not isostructural to **2c**. In a control experiment, grinding $ZnCl_2$ and TPT in a 3:2 molar ratio and then heating to 573 K for 60 h did not produce **3a** but rather **3b** as shown by XRPD. This was further supported by TG-DSC analysis in which again a grinding mixture of a 3:2 metal-to-ligand ratio showed an exothermic peak at ca. 553 K as a result of the crystallization of **3b** (Figure S22).[44]

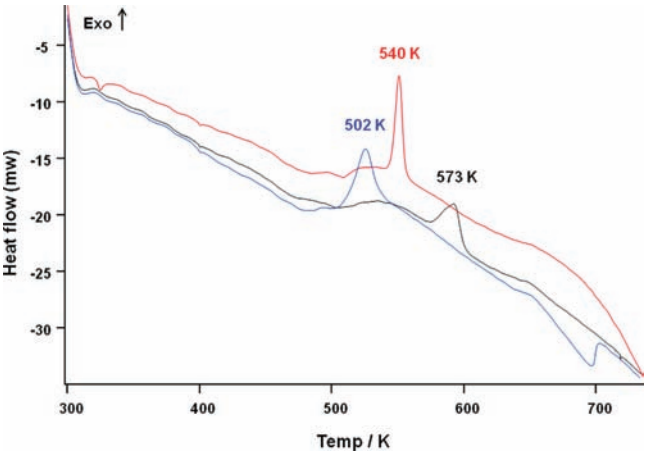

Figure 11. Comparison of DSC of **1** (black), **2** (red), and **3** (blue). Crystallization of **1a**, **2a**, and **3b** occurs after the formation of the amorphous phase and is clearly observed by the exothermic peaks at 573, 540, and 502 K, respectively, where the temperatures indicate the rising rather than the peak top positions.

The Influence of Zinc Halides in the Solid-State Reaction of Interpenetrated Porous Networks. Upon heating, each interpenetrated porous network **1**, **2**, and **3** initially produces amorphous phases. However, interestingly, if heating continues, network **1** converts into a noninterpenetrated network (**1a**), whereas networks **2** and **3** give interpenetrated networks **2a** and **3a**, respectively. Even though once periodicity of frameworks is lost at 473 K, surprisingly further heating produces new thermally stable crystalline phases. Metastable networks **1**, **2**, and **3** are isostructural and contain the same solvent. Therefore, the different crystal structures **1a** and **2a** can be rationalized due to the presence of different zinc halides. To better understand this aspect, we compared the DSC experiments of **1**, **2**, and **3** upon heating from 300 to 725 K (Figure 11). The removal of solvent molecules takes place at 300−473 K, followed by the formation of the amorphous phase (i.e., corroborated by XRPD) and crystallization as denoted by the exothermic peaks at 573 and 540 K corresponding to **1a** and **2a**, respectively. Importantly, the two exothermic peaks appear at different temperatures, indicating that higher energy is required to form **1a** than **2a**. Thus, after the amorphous phase formation, different reorganization processes such as bond-breaking and bond-forming can occur and hence may explain the different structures of **1a** and **2a**. In case of **3**, the desolvated structure **3a** was unstable and thus directly transformed to **3b**. These reactivity differences can be attributable to the different strength of coordination bonds between Zn and halide atoms.

CONCLUSIONS

Through our studies, we determined that **1**, **2**, and **3** differ in the solid-state reactivity at elevated temperatures while having in common the same interpenetrated topology and crystal-to-amorphous-to-crystal transformations. As a result, three new structures with different topology were obtained upon heating. We hypothesized that these differences are attributable to the different strength of coordination bonds between Zn and halide atoms. Importantly, those networks can not be prepared from the solid-state reactions of each starting material, ZnX_2 (X = I, Br, Cl) and TPT. This leads us to conclude that the initial arrangement of the building units in the interpenetrated structures is a critical

factor influencing the reaction trajectory, suggesting that perhaps a sort of "memory effect" exists in the described phase transitions for transferring structural information between structures. Although the results reported in this paper are for a particular family of isostructural porous coordination networks (10,3-*b*), we believe that the process can be applied to other materials to prepare a new class of solids. Meanwhile, *ab initio* powder X-ray diffraction determination will be a very powerful analytical tool. We anticipate that the strategy reported here will be widely adopted, thus, contributing to the progress in materials science.

EXPERIMENTAL SECTION

X-ray Powder Diffraction Data. High quality powder X-ray diffraction pattern for compounds **1a**·$\mathbf{G_1}$ and **2a** were recorded at 83 and 100 K, respectively, in transmission mode [0.3 mm capillary; synchrotron radiation λ = 0.9948 Å; 2θ range = 3−60°; step width = 0.01°; data collection time 20 min for **1a**·$\mathbf{G_1}$ and λ = 1.3 Å; 2θ range = 4−68°; step width = 0.01°; data collection time 30 min for **2a**] on a diffractometer equipped with a blue imaging plate detector at SPring-8 BL19B2 and BL02B2 beamlines.

***Ab Initio* Structure Determination.** Details of the structure determination of **1a** have been reported elsewhere.[28] The XRPD pattern of **1a**·$\mathbf{G_1}$ and **2a** were indexed using the program DICVOL.[45] The structure determination was carried out by the simulated annealing method with the program DASH.[46] The Rietveld refinements were performed with programs RIETAN-FP[47] and VESTA.[48] Restraints but no constraints for all bond lengths were employed to maintain the molecular geometry. Thermal temperature factors were refined isotropically and uniform values were applied to the framework. The details of the *ab initio* structure determinations are in the Supporting Information section.

Single Crystal X-ray Structure Determination of 2c and 3b. The diffraction data for **2c** and **3b** were recorded with a Bruker APEX-II/CCD diffractometer equipped with a focusing mirror (Mo Kα radiation, λ = 0.71073 Å) with a cryostat system equipped with an N_2 generator (Japan Thermal Eng. Co., Ltd.). Crystal data for **2c**: $C_{18}H_{12}Br_4N_6Zn_2$, M_r = 762.72, crystal dimensions 0.02 × 0.02 × 0.01 mm^3, orthorhombic, space group, *Pbca*, unit cell, a = 17.339(6), b = 14.752(6), c = 18.507(7) Å, V = 4734(3) Å^3, T = 85 K, Z = 8, 4942 unique reflections out of 5992 with $I > 2\sigma(I)$, 271 parameters, 2.12 < θ < 28.91°, final R factors R_1 = 0.0220 and wR_2 = 0.0483.

Crystal data for **3b**: $C_{18}H_{12}Cl_4N_6Zn_2$, M_r = 584.88, crystal dimensions 0.02 × 0.02 × 0.01 mm^3, monoclinic, space group, $P2_1/n$, unit cell, a = 11.759(4), b = 9.403(3), c = 19.364(7) Å, β = 100.515(4)°, V = 2105.2(13) Å^3, T = 85 K, Z = 4, 3313 unique reflections out of 5146 with $I > 2\sigma(I)$, 271 parameters, 1.89 < θ < 28.78°, final R factors R_1 = 0.0445 and wR_2 = 0.0847.

Single Crystal X-ray Structure Determination of 3c. Data diffraction of **3c** was collected at Pohang Accelerator Laboratory (beamline 6B1, λ = 0.88559 Å).

Crystal data for **3c**: $C_{72}H_{55}Cl_6N_{18}O_{12}Zn_3$, M_r = 1772.14, crystal dimensions 0.10 × 0.04 × 0.04 mm^3, orthorhombic, space group, *Fdd*2, unit cell, a = 49.6200(1), b = 50.5890(6), c = 6.0590(6) Å, V = 15209.5(15) Å^3, T = 90 K, Z = 8, 4010 unique reflections out of 4491 with $I > 2\sigma(I)$, 456 parameters, 2.05 < θ < 28.76°, final R factors R_1 = 0.0792 and wR_2 = 0.2152.

ASSOCIATED CONTENT

Supporting Information. Synthetic details, elemental analyses, TG-DSC, XRPD patterns, and crystallographic details (CIF; also see CCDC entries 781948−781953). This material is available free of charge via the Internet at http://pubs.acs.org.

AUTHOR INFORMATION

Corresponding Author
mkawano@postech.ac.kr

Present Addresses
[#]Italian Institute of Technology, Centre for Nano Science and Technology (CNST-IIT@PoliMi), Via Pascoli 70/3, 20133 Milan, Italy.

ACKNOWLEDGMENT

This research was supported by WCU (World Class University) program through the Korea Science and Engineering Foundation funded by the Ministry of Education, Science and Technology (Project No R31-2008-000-10059-0). We thank the Japan Society for the Promotion of Science (fellowship to J.M.-R.) for funding. This work was approved by SPring-8 (Proposals 2008A1843 and 2008A1938). Single crystal and powder X-ray diffraction experiments were performed at the Pohang Accelerator Laboratory (beamlines 6B1 and 8C2) supported by Pohang University of Science and Technology.

REFERENCES

(1) Batten, S. R.; Robson, R. *Angew. Chem., Int. Ed.* **1998**, *37*, 1460–1494.
(2) Eddaoudi, M.; Moler, D. B.; Li, H.; Chen, B.; Reineke, T. M.; O'Keeffe, M. O.; Yaghi, O. M. *Acc. Chem. Res.* **2001**, *34*, 319–330.
(3) Moulton, B.; Zaworotko, M. J. *Chem. Rev.* **2001**, *101*, 1629–1658.
(4) Kitagawa, S.; Kitaura, R.; Noro, S. *Angew. Chem., Int. Ed.* **2004**, *43*, 2334–2375.
(5) Férey, G. *Chem. Soc. Rev.* **2008**, *37*, 191–214.
(6) Wang, B.; Côté, A. P.; Furukawa, H.; O'Keeffe, M.; Yaghi, O. M. *Nature* **2008**, *453*, 207–211.
(7) Férey, G.; Millange, F.; Morcrette, M.; Serre, C.; Doublet, M. L.; Grenèche, J. M.; Tarascon, J. M. *Angew. Chem., Int. Ed.* **2007**, *46*, 3259–3263.
(8) Fujita, M.; Kwon, Y. J.; Washizu, S.; Ogura, K. *J. Am. Chem. Soc.* **1994**, *116*, 1151–1152.
(9) Matsuda, R.; Kitaura, R.; Kitagawa, S.; Kubota, Y.; Belosludov, R. V.; Kobayashi, T. C.; Sakamoto, H.; Chiba, T.; Takata, M.; Kawazoe, Y.; Mita, Y. *Nature* **2005**, *436*, 238–241.
(10) Philp, D.; Stoddart, J. F. *Angew. Chem., Int. Ed. Engl.* **1996**, *35*, 1154–1196.
(11) Lehn, J.-M. *Chem. Soc. Rev.* **2007**, *36*, 151–160.
(12) Fujita, M. *Chem. Soc. Rev.* **1998**, *27*, 417–425.
(13) Kawano, M.; Fujita, M. *Coord. Chem. Rev.* **2007**, *251*, 2592–2605.
(14) Haneda, T.; Kawano, M.; Kawamichi, T.; Fujita, M. *J. Am. Chem. Soc.* **2008**, *130*, 1578–1579.
(15) Das, S.; Kim, H.; Kim, K. *J. Am. Chem. Soc.* **2009**, *131*, 3814–3815.
(16) Kawamichi, T.; Haneda, T.; Kawano, M.; Fujita, M. *Nature* **2009**, *461*, 633–635.
(17) Martí-Rujas, J.; Matsushita, Y.; Izumi, F.; Fujita, M.; Kawano, M. *Chem. Commun.* **2010**, *46*, 6516–6517.
(18) Harris, K. D. M.; Tremayne, M.; Lightfoot, P.; Bruce, P. G. *J. Am. Chem. Soc.* **1994**, *116*, 3543–3547.
(19) Harris, K. D. M.; Cheung, E. Y. *Chem. Soc. Rev.* **2004**, *33*, 526–538.
(20) Harris, K. D. M.; Tremayne, M.; Kariuki, B. *Angew. Chem.* **2001**, *113*, 1674–1700; *Angew. Chem., Int. Ed.* **2001**, *40*, 1626–1651.
(21) Guo, F.; Martí-Rujas, J.; Pan, Z.; Hughes, C. E.; Harris, K. D. M. *J. Phys. Chem. C.* **2008**, *112*, 19793–19796.

(22) Martí-Rujas, J.; Morte-Ródenas, A.; Guo, F.; Thomas, N.; Fujii, K.; Kariuki, B. M.; Harris, K. D. M. *Crys. Growth Des.* **2010**, *10*, 3176–3181.
(23) Pagola, S.; Stephens, P. W.; Bohle, D. S.; Kosar, A. D.; Madsen, S. K. *Nature* **2000**, *404*, 307–310.
(24) Férey, G.; Mellot-Draznieks, C.; Serre, C.; Millange, F.; Dutour, J.; Surblé, S.; Margiolak, I. *Science* **2005**, *309*, 2040–2042.
(25) *Structure Determination from Powder Diffraction Data*; David, W. I. F., Shankland, D., McCusker, L. B., Baerlocher, C., Eds.; IUCr Monographs on Crystallography *13*; Oxford University Press: Oxford, U.K., 2002.
(26) Izumi, F. *The Rietveld Method*; Oxford University Press: Oxford, U.K., 1995.
(27) Cohen, M. D.; Schmidt, G. M.; Flavian, S. *J. Chem. Soc.* **1964**, 2041–2051.
(28) Ohara, K.; Martí-Rujas, J.; Haneda, T.; Kawano, M.; Hashizume, D.; Izumi, F.; Fujita, M. *J. Am. Chem. Soc.* **2009**, *131*, 3860–3861.
(29) Kawano, M.; Haneda, T.; Hashizume, D.; Izumi, F.; Fujita, M. *Angew. Chem., Int. Ed.* **2008**, *47*, 1269–1271.
(30) Robson et al. reported the network **3** without detailed information in reference.[1] We attempted to redetermine the crystal structure in this study using single crystal X-ray diffraction, but high quality data was not obtained due to polycrystallinity. However, we determined the 10,3-*b* type framework (see ref 42). Our X-ray powder diffraction experiments, TG-DSC, and elemental analysis suggest that the product **3** is the same interpenetrated network as **1** and **2**. Therefore, we used **3** as a starting material for the heating experiment.
(31) Delgado-Friedrichs, O.; O'Keeffe, M.; Yaghi, O. M. *Acta Crystallogr., Sect. A* **2003**, *59*, 515–525.
(32) Biradha, K.; Fujita, M. *Angew. Chem., Int. Ed.* **2002**, *41*, 3392–3395.
(33) For the details of the *ab initio* structure determination at 95 K (vacuum), and structural information, see Supporting Information.
(34) Due to experimental conditions, the XRPD of **1a**·$\mathbf{G_1}$ and **1a** were collected at different temperatures 95 K (vacuum) and 82 K.
(35) Cavallo, G.; Metrangolo, P.; Pilati, T.; Resnati, G.; Sansotera, M.; Terraneo, G. *Chem. Soc. Rev.* **2010**, *39*, 3772–3783.
(36) Rimmer, E. L.; Bailey, R. D.; Hanks, T. W.; Pennington, W. T. *Chem.—Eur. J.* **2000**, *6*, 4071–4081.
(37) Metrangolo, P.; Neukirch, H.; Pilati, T.; Resnati, G. *Acc. Chem. Res.* **2005**, *38*, 386–395.
(38) Caronna, T.; Liantonio, R.; Logothetis, T. A.; Metrangolo, P.; Pilati, T.; Resnati, G. *J. Am. Chem. Soc.* **2004**, *126*, 4500–4501.
(39) Metrangolo, P.; Meyer, F.; Pilati, T.; Resnati, G.; Terraneo., G. *Angew. Chem., Int. Ed.* **2008**, *47*, 6114–6127.
(40) Ohmori, O.; Kawano, M.; Fujita, M. *Angew. Chem. Int. Ed.* **2005**, *44*, 1962–1964. **1b** has an interpenetrated structure in which triphenylene is intercalated between two triazine ligands. Triphenylene is regarded as a host framework rather than guest because it cannot be replaced by common aromatic compounds under guest exchange conditions, due to the strong stacking between triazine panels and triphenylene thorough charge-transfer interactions.
(41) See Supporting Information to see the XRPD pattern of **2a** obtained after heating **2** and **2b** at 553 K (Figure S10). We also obtained the same XRPD pattern and hence the same interpenetrated structure **2a** from a biporous coordination network reported in ref 29 (Figure S11).
(42) As explained in ref 30, **3** has the same topology of **1** and **2**. We managed to obtain the crystal structure of **3** using single crystal X-ray diffraction and, although we could not locate the nitrobenzene molecules, we did determine the framework (Figure S16) and simulate the XRPD pattern. Figure S17 shows the comparison between the experimental and simulated XRPD patterns. Slow layer-to-layer diffusion method with the same stoichiometry of starting reagents produced single crystals of the 3D network structure $[(ZnCl_2)_3(TPT)_2]_n \cdot 6(C_6H_5NO_2)$ (**3c**) although **3** can be obtained as a minor product. The network **3c** has 1D channels formed by $\pi-\pi$ stacking of TPT (Figure S24). See Supporting Information for detailed information.
(43) Compound **3** did not provide a clear XRPD pattern after reaching 573 K, whereas compounds **1** and **2** having good crystallinity provided **1a** and **2a** via crystalline-to-amorphous-to-crystalline (CAC) transformation at 573 K. In the case of **3**, the equivalent **3a** obtained after the amorphous phase is not crystalline enough and cannot be characterized by *ab initio* X-ray diffraction. However, similarities with the diffraction pattern of **2a** and elemental analyses suggest the same desolvated structure.
(44) We note that the temperature difference in the exothermic peaks obtained after heating **3** (525 K) and after heating a grinding mixture of $ZnCl_2$ and TPT (553 K) can be rationalized by the presence of nitrobenzene in **3**. In the case of $ZnCl_2$, since it is very likely that solid—liquid phase was created at 573 K, the most stable product **3b** was obtained.
(45) Boultif, A.; Louër, D. *J. Appl. Crystallogr.* **1991**, *24*, 987–993.
(46) David, W. I. F.; Shankland, K; van de Streek, J; Pidcock, E; Motherwell, W. D. S.; Cole, J. C. *J. Appl. Crystallogr.* **2006**, *39*, 910–915.
(47) Izumi, F.; Momma, K. *Solid State Phenom.* **2007**, *130*, 15–20.
(48) Momma, K.; Izumi, F. *J. Appl. Crystallogr.* **2008**, *41*, 653–658.